

Spatiotemporal Self-Assembly of Peptide Amphiphiles by Carbonic Anhydrase IX-Targeting Induces Cancer-Lysosomal Membrane Disruption

Dohyun Kim,[‡] Sangpil Kim,[‡] Gaeun Park, Huyeon Choi, and Ja-Hyoung Ryu^{*}



Cite This: *JACS Au* 2022, 2, 2539–2547



Read Online

ACCESS |

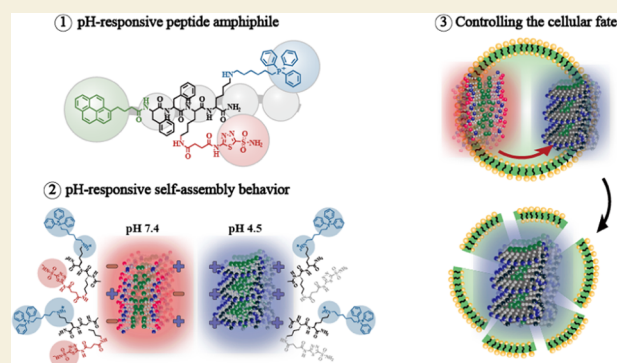
Metrics & More

Article Recommendations

Supporting Information

ABSTRACT: To achieve spatiotemporal control, an enzyme-instructed self-assembly system is widely used, but this approach typically has a small effect on cellular fate. In this study, we show that the intralysosomal assembly by a carbonic anhydrase IX (CAIX)-targeting peptide amphiphile (Pep-AT) can control cellular fate with a low therapeutic dose by tuning the surface charge based on pH change. Pep-AT self-assembles into a fibrous aggregate with a negative surface charge in an extracellular environment near CAIX. During endocytosis, it changes into a nanofiber with a positive surface charge at the lysosome. Then, it can disrupt the lysosomal membrane and induce cellular apoptosis. This study demonstrates that a spatiotemporal assembly induced by a cancer enzyme and specific organelle can control the cellular fate of cancer.

KEYWORDS: peptide self-assembly, pH dependent, lysosome, enzyme targeting, supramolecular chemistry



In nature, cellular organelles independently regulate their internal pH to properly perform cellular processes.^{1–4} The biomacromolecules of each organelle generally require the optimal pH level for the function. For example, cathepsins, which are lysosomal peptidases, are present in the form of inactive proenzymes at physiological pH. However, they undergo conformational change for generating catalytic activity in response to low pH at the lysosome.^{5–8} Owing to the nature of being activated in an appropriate environment, biomacromolecules are less active and do not affect surrounding cellular processes in an aberrant subcellular location.^{9–11} Inspired by the process of nature, many artificial systems, which are activated in the desired environment, are being developed to regulate cellular processes while minimizing the impact on surrounding cells.^{12–15} For this strategy, it is essential to spatiotemporally localize the artificial system into the desired location. In recent years, enzyme-instructed self-assembly strategies have been developed to achieve precise spatiotemporal control of nanostructures inside cells. For instance, a short peptide that has a cleavage moiety by a specific enzyme (i.e., ALP, furin, SIRT, and MMP) has been demonstrated with the change in hydrophilic–lipophilic balance, resulting in the formation of a nanostructure in an extracellular membrane, cytosol, or specific organelle.^{16–20} It has been used to modulate cell behavior by sequestering intracellular protein, modifying the biomacromolecule structure (e.g., DNA methylation), or regulating the cellular environment (e.g., elevated reactive oxygen species). Although these systems

suggest a potential to modulate cellular processes, there are still limitations to the spatiotemporal control of dynamic cellular milieu, such as cellular organelle.

One of the efficient approaches to controlling cellular fate is to regulate organelle membrane integrity using peptide self-assembly. Organelle membranes perform various metabolic processes through a membrane-bound receptor and channel protein, which regulate the transportation of ions, nutrients, wastes, and metabolic products.^{21,22} Therefore, a system that disturbs the membrane integrity can effectively control cellular mortality and have the potential for anticancer therapy. To disturb the cell membrane integrity, peptide amphiphiles (PAs) consisting of cationic and hydrophobic sequences have been widely exploited.²³ The cell membrane has a negative charge attributed to the glycoprotein and polysaccharide chain and a hydrophobic bilayer structure. Thus, a presentation of the highly lipophilic and positive surface of the self-assembled nanostructures can efficiently interact with the cell membrane or organelle membrane through electrostatic and hydrophobic interactions, as followed by agitating the membrane integrity.

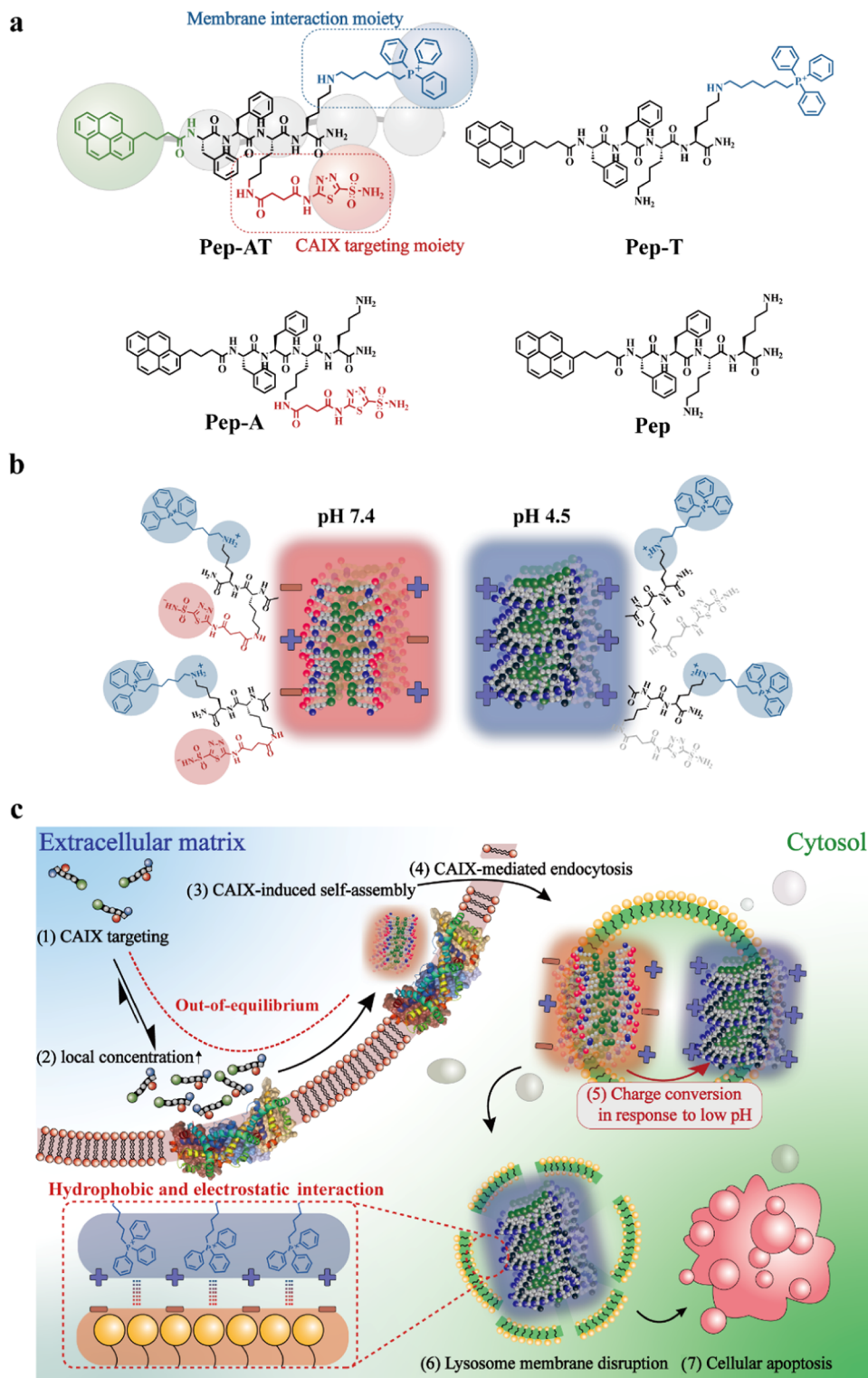
Received: July 29, 2022

Revised: October 24, 2022

Accepted: October 24, 2022

Published: November 1, 2022



Scheme 1. Schematic Illustration Showing the Mechanism of Pep-AT^a

^a(a) Molecular structure of Pep-AT and its negative control groups. Pep-AT is functionalized by acetazolamide and TPP. (b) Schematic illustration showing the self-assembly behavior of a pH-controllable peptide. Surface charge can be tuned on the basis of pH, and the self-assembly propensity can be changed. (c) Application of controllable peptides at the cellular level. The strong binding affinity between acetazolamide and CAIX can provide the targeting ability toward CAIX on the cancerous membrane. The local concentration around CAIX increases over time toward an out-of-equilibrium state. After reaching the concentration above CAC, the CAIX-induced self-assembly nanostructure can be spatiotemporally formed on an extracellular membrane. The nanofiber can be internalized into lysosomes via CAIX-mediated endocytosis, and charge conversion occurs in response to lysosomal pH. Increased interaction with the lysosomal membrane can disturb membrane integrity, and cellular apoptosis can occur.

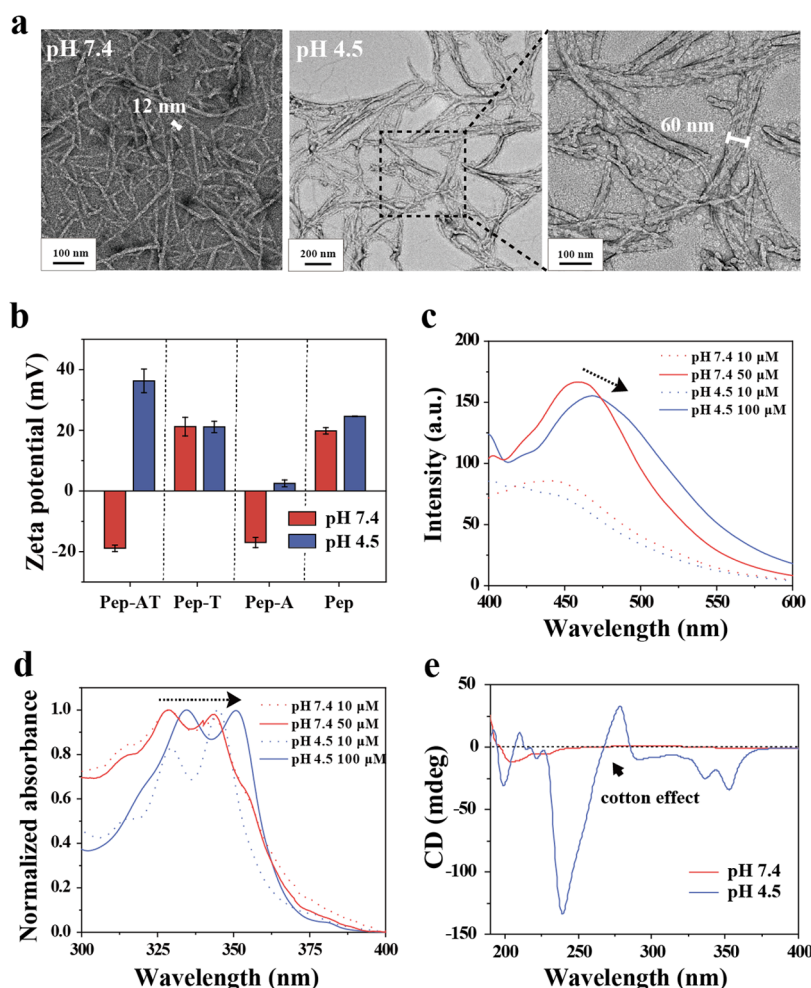


Figure 1. pH-dependent self-assembly behavior study. (a) TEM image of Pep-AT at pH 4.5 and pH 7.4 (scale bar = 200 nm), and its magnified image (scale bar = 100 nm). (b) Surface charge observation using a Zeta-sizer; 50 μ M of the Pep-AT was prepared at pH 7.4, and the other group was prepared at 100 μ M. Data are presented as mean \pm SD ($n = 3$). (c) Fluorescence intensity of Pep-AT before and after self-assembly at pH 7.4 and pH 4.5. (d) Normalized ultraviolet–visible (UV–vis) absorbance of Pep-AT before and after self-assembly at pH 7.4 and pH 4.5. (e) Circular dichroism (CD) spectroscopy for Pep-AT in 50 μ M at pH 7.4 and 100 μ M at pH 4.5.

Recently, Stupp et al. have reported that the cohesive force from the positively charged bioactive epitope of nanofibers can serve as a membrane-disrupting agent contributing to cell toxicity.²⁴ Additionally, our group has demonstrated that the formation of nanostructures containing a lipophilic and cationic triphenylphosphonium (TPP) moiety can induce cell death by disrupting the mitochondrial membrane integrity.^{25,26} However, the positive charge of the molecules can induce undesired cytotoxicity in a normal healthy cell. Thus, there is an unmet need to regulate cellular fate by spatiotemporally activating a positively charged bioactive epitope only within the desired organelles.

In this study, we demonstrate that enzyme-targeted self-assembly can disrupt the cancer-lysosomal membrane via charge reversal of the nanostructure, depending on the pH (Scheme 1). The assembly is induced in the cellular membrane where the target enzyme (carbonic anhydrase IX, CAIX) is located, and during endocytosis, the assembly is trapped inside the lysosome. Decreasing the pH value changes the surface charge of the peptide assembly from negative to positive, which results in lysosomal membrane disruption, thereby directly inducing cellular apoptosis. We designed a tetrapeptide consisting of Phe–Phe–Lys–Lys, which has a potential self-

assembly propensity (Scheme 1a). To add specific functions, we functionalized this sequence with acetazolamide and TPP in each lysine residue (peptide amphiphile (Pep-AT)). Since the pK_a of acetazolamide is approximately 7.2,²⁷ the self-assembly of the peptide can be tuned depending on the pH (Scheme 1b). At the cellular level, Pep-AT can target CAIX based on its strong affinity with acetazolamide (Scheme 1c). In particular, CAIX is overexpressed in many cancerous membranes.^{28–30} Thus, we have observed that our peptide can selectively self-assemble around the cancer membrane. The generated nanofibers can be encapsulated into lysosomes during CAIX-mediated endocytosis; thus, the skeleton of nanofibers can be changed in response to the lysosome environment. The high positive charge, because of the disappearance of the negative charge by the reprotonation of the deprotonated acetazolamide in the acidic lysosome, and the lipophilicity of the TPP of the self-assembled nanostructure, can strongly interact with the lysosomal membrane, disrupting the membrane integrity and directly inducing cellular apoptosis. Owing to this direct and significant interaction with the lysosomal membrane, this system shows high therapeutic efficiency, inducing cellular apoptosis and the

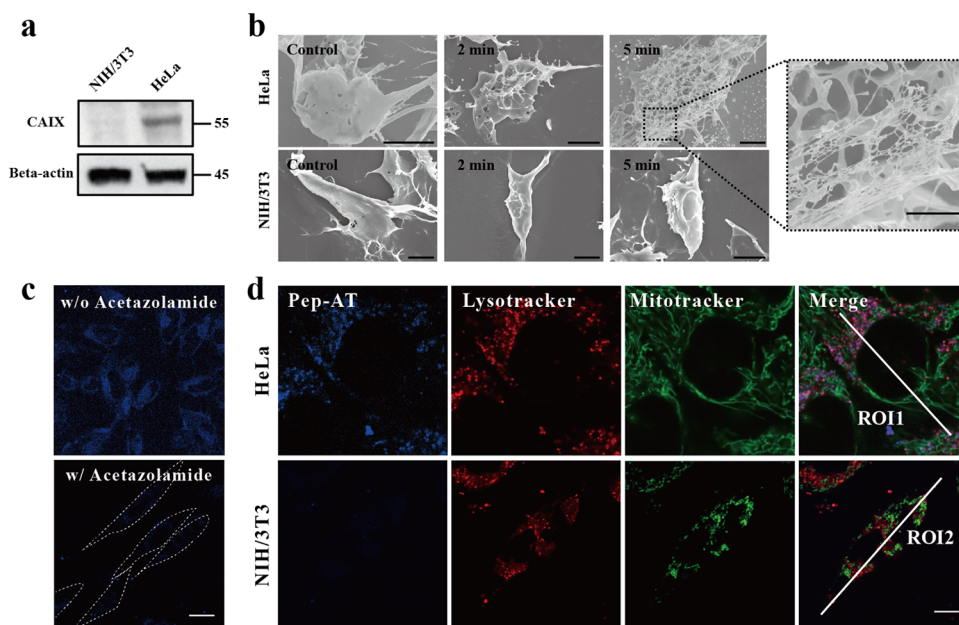


Figure 2. CAIX-induced self-assembly behavior and lysosome accumulation study. (a) Western blotting image showing the degree of expression level for CAIX in HeLa and NIH/3T3. (b) Time-dependent SEM image after treatment of 20 μM Pep-AT toward HeLa and NIH/3T3 (scale bar = 1 μm), and its magnified image (scale bar = 4 μm). (c) CLSM image after incubation of 20 μM Pep-AT for 10 min toward control HeLa and HeLa with acetazolamide for the competition assay to check the cellular uptake (scale bar = 20 μm). (d) Colocalization study of Pep-AT with LysoTracker Red and Mitotracker Green after 20 μM treatment of Pep-AT for 30 min in HeLa and NIH/3T3 (scale bar = 4 μm).

potential for anticancer therapy without additional chemotherapy.

The peptide backbone (Pyrene–Phe–Phe–Lys–Lys) with the purpose of self-assembly was prepared via solid-phase peptide synthesis. Afterward, TPP was conjugated to the peptide backbone to increase the membrane interaction ascribed to the lipophilic and positive-charge properties. Finally, acetazolamide, which plays an essential role in targeting the CAIX enzyme,^{28–30} was attached to afford Pep-AT. The detailed synthesis and characterization of the corresponding peptides are demonstrated in the Supporting Information (Scheme S1, Figures S1–S11). As control peptides, we prepared Pep-T without acetazolamide to prove the CAIX-targeting potential, Pep-A without TPP to evaluate the function of TPP, and Pep without functional ligands.

We initially explored the self-assembly behaviors of each peptide in vitro. We prepared a 100 μM solution in phosphate-buffered saline (PBS) at pH 7.4, and the supramolecular structure was studied by transmission electron microscopy (TEM). As demonstrated in Figures S12 and 1a, a nanofiber was observed for Pep-AT, Pep-A, Pep-T, and Pep, and its diameters were approximately 12, 15, 52, and 8 nm, respectively. To analyze the self-assembly behavior in detail, we measured the critical aggregation concentration (CAC) using pyrene as a probe. The CAC values were determined to be 28, 32, 52, and 77 μM for Pep-AT, Pep-A, Pep-T, and Pep, respectively (Figure S13). Notably, Pep-AT and Pep-A showed comparable CAC values because both were present in the zwitterionic form at pH 7.4. However, Pep-T and Pep, which possessed an intrinsic positive charge at pH 7.4, exhibited higher CAC than Pep-AT and Pep-A. Our observation implied that the self-assembly propensity was changed depending on the molecular structure, which can trigger the alteration for molecular interaction of the peptide building block.^{31–33} Additionally, Pep-AT exhibits different molecular charges

depending on pH since acetazolamide would be fully protonated at low pH, attributed to the pK_a value of sulfonamide ($pK_a \sim 7.2$).²⁷ Therefore, we postulated that the self-assembly propensity for Pep-AT varied in response to pH with the molecular charge transition. This led us to envision that lysosome, which possesses low pH in a cellular environment, is an attractive target in cells to vary the self-assembly behavior.

Accordingly, we investigated the pH-dependent self-assembly behavior at pH 4.5 and pH 7.4. Initially, we measured the CAC at pH 4.5, showing 12 μM (Figure S14). It decreases compared to pH 7.4, indicating the self-assembly propensity changed at pH 4.5. To prepare a self-assembly solution, we set out a 100 μM solution, which is above the CAC, while a 50 μM solution was prepared at pH 7.4 due to the aggregation problem. Then, we performed the surface analysis of the self-assembly structure using a Zeta-sizer. We observed the surface charge conversion from negative charge to positive charge for Pep-AT and Pep-A, depending on pH (Figure 1b). Intriguingly, the amount of charge conversion for Pep-AT was higher than that for Pep-A, postulated by the evidence of the high positive charge from TPP. However, we observed a constant amount of charge at pH 7.4 and pH 4.5 for Pep-T and Pep, indicating that the absence of acetazolamide exhibits the loss of self-assembly tunability depending on pH. Overall, these results indicate that the surface charge for the self-assembly structure derived from Pep-AT can be changed depending on pH.

Subsequently, we evaluated the pH-dependent self-assembly behavior in detail by spectroscopy.^{34,35} To get a closer look at the molecular packing, we first measured fluorescence spectroscopy. It showed a bathochromic shift for a pyrene excimer peak at 460 nm ($\lambda_{\text{ex}} = 360$ nm) in pH 4.5 (Figure 1c). Likewise, we observed a bathochromic shift for the pyrene absorbance maxima only at pH 4.5 (Figure 1d). These results

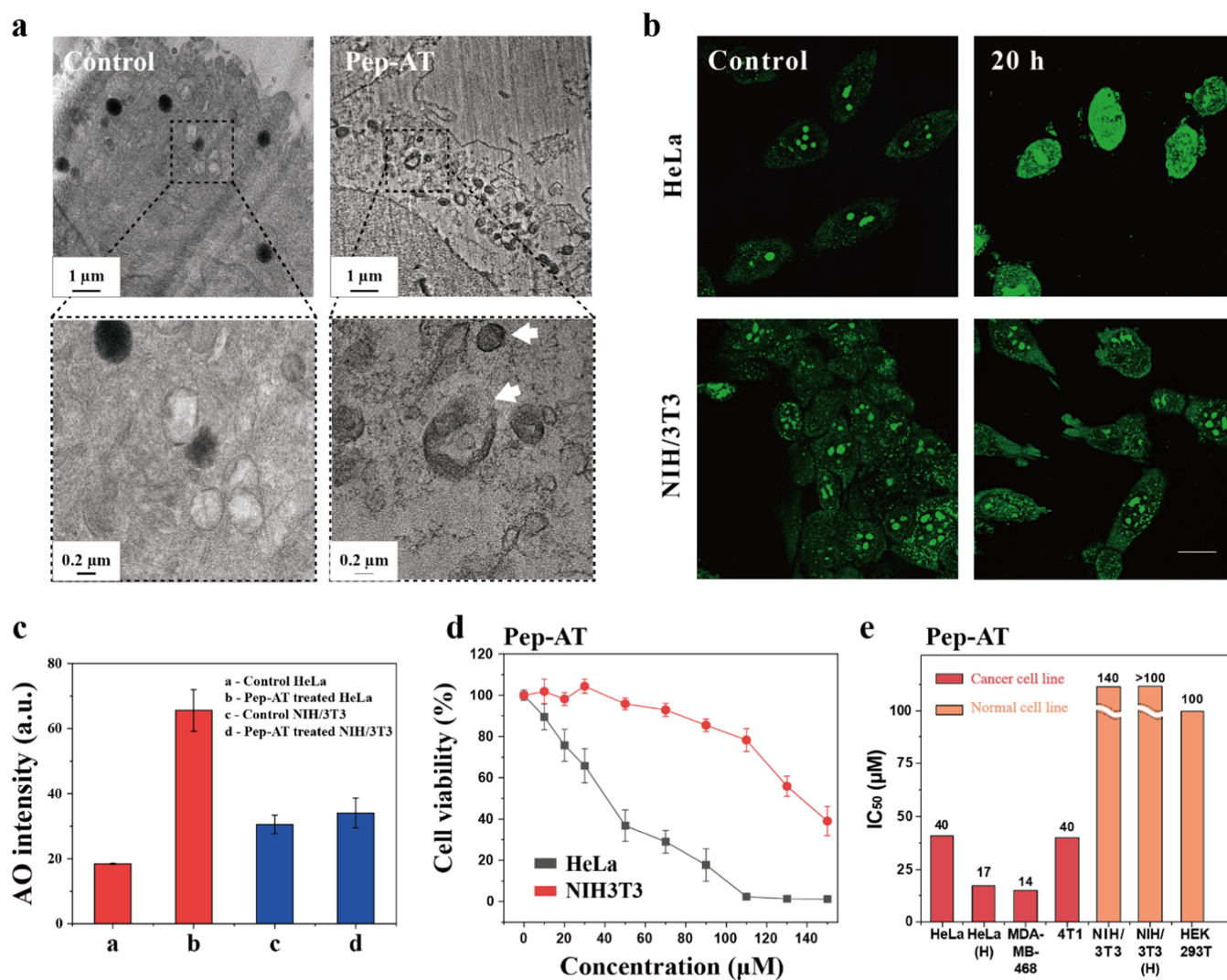


Figure 3. Lysosomal membrane integrity study and cell viability assay to explore the potential of Pep-AT for cancer therapy. (a) TEM image for control HeLa and HeLa after treatment using 20 μM Pep-AT to observe the nanofibers inside the lysosome (scale bar = 1 μm), and its magnified image (scale bar = 0.2 μm); white arrows indicate the lysosomal membrane swelling. (b) CLSM image of acridine orange (AO) dye after treatment of 20 μM Pep-AT for 20 h to observe the lysosomal membrane integrity of HeLa and NIH/3T3 (scale bar = 20 μm). (c) Fluorescence intensity of the AO dye between the Pep-AT-treated and the control group was plotted. (d) Cell viability of Pep-AT toward HeLa (black line) and NIH/3T3 (red line) was measured under the normoxia condition by an MTT assay. (e) IC₅₀ value of Pep-AT after 24 h incubation was measured against the cancer cell line (red bar) and the normal cell line (orange bar). The data labels in the bar graph indicate the IC₅₀ value. (H) represents hypoxia condition. Data are presented as mean \pm SD ($n = 3$).

suggested the formation of a supramolecular J-aggregate at pH 4.5 with surface charge transition. Next, to obtain further insight into the internal structure, we carried out circular dichroism (CD) spectroscopy according to pH.³⁵ We observed a strong positive cotton effect for TPP and a negative band for pyrene at pH 4.5, while no signal was observed at pH 7.4 (Figure 1e). The chirality change depending on pH was not derived from the chirality of the monomer, which was further confirmed by the CD spectra in a diluted solution (10 μM at both pH) (Figure S15). This finding showed that the chiral internal structure was generated at pH 4.5 with surface charge transition. Further, we observed the nanofiber morphology at pH 4.5 using TEM. The nanofiber with a diameter of up to 60 nm was observed, showing an increased diameter compared to pH 7.4 (Figure 1a). It indicates that the internal secondary structure transition at pH 4.5 affected the morphology of the

nanofiber. Overall, the results indicate that the self-assembly propensity of Pep-AT can be changed depending on the pH.

Generally, acetazolamide serves as a targeting moiety for CAIX, which is commonly overexpressed in many cancerous cells, thereby providing an attractive anticancer target.^{28–30} Interestingly, we observed nanofiber generation in HeLa cancer cells, while there was no assembly near an NIH/3T3 normal cell. This indicates that Pep-AT can preferentially accumulate near CAIX, and the local concentration can significantly increase to spatiotemporally generate a self-assembly nanofiber. The CAIX expression level was confirmed by western blot analysis, showing that HeLa exhibited a 3-fold higher expression level than NIH/3T3 (Figures 2a and S16). Thereafter, we observed the cell surface by scanning electron microscopy (SEM) in a time-dependent manner. After incubating 20 μM Pep-AT into HeLa, a nanofiber was observed at 2 min on the HeLa cell surface, while only a

smooth cell surface was observed in the control HeLa (Figure 2b). Moreover, the size of the nanofibers covering the cell surface increased at 5 min, postulating that the local concentration gradually increased toward CAIX, resulting in a dissipative out-of-equilibrium supramolecular structure.³⁶ Conversely, no significant nanofiber was generated in NIH/3T3 up to 5 min, and NIH/3T3 appeared to be identical to the control group. The overall results indicated that Pep-AT could be self-assembled on a cancer cell that generally overexpressed CAIX, while little targeting ability for the normal cell was observed.

Subsequently, we examined CAIX-mediated endocytosis into the lysosome for Pep-AT. First, 20 μ M Pep-AT was incubated into HeLa, and we observed blue fluorescence inside the cells after 10 min using confocal laser scanning microscopy (CLSM) (Figure 2c), indicative of endocytosis of the Pep-AT. To prove the relevance to the CAIX for cellular uptake, a competition assay using a small molecular inhibitor (i.e., acetazolamide) was conducted. In the presence of an excess amount of acetazolamide (200 μ M), we observed that the blue fluorescence of Pep-AT was significantly reduced. This result suggests that CAIX-mediated endocytosis is relevant for the cell entry mechanism of Pep-AT. Then, we performed a colocalization study using an organelle tracker dye (LysoTracker Red and Mitotracker Green) to investigate the localization of Pep-AT inside cells. In the CLSM image, we observed a colocalized signal with blue fluorescence for Pep-AT and red fluorescence for LysoTracker Red in 20 μ M Pep-AT-treated HeLa for 30 min (Figure 2d). Further, colocalization was confirmed by fluorescence-intensity profile analysis, where peak overlap between the blue and red signals was observed (Figure S17). We treated Pep-AT into HeLa with increased incubation times (4 and 24 h) to determine whether Pep-AT could target other cellular organelles. CLSM images showed that colocalization with LysoTracker Red was observed at 4 h incubation (Figure S18). At 24 h incubation, Pep-AT still existed in the lysosome before entering the cell death pathway. In contrast, blue fluorescence was not observed in NIH/3T3, indicating that the accumulation of Pep-AT in the lysosome significantly decreased due to the lack of CAIX expression. This result suggests that Pep-AT could be spatiotemporally localized into cancerous lysosomes via CAIX targeting.

Additionally, we synthesized NBD-AT conjugated with nitrobenzofurazan (NBD) instead of pyrene at the N-terminal (Figures S10 and S11) to quantitatively analyze the cellular uptake between HeLa and NIH/3T3. We incubated 20 μ M NBD-AT into HeLa and NIH/3T3, followed by performing cell lysis to obtain the overall fluorescence in the cells. Figure S19 shows that the fluorescence intensity from HeLa is 3.5-fold higher than that from NIH/3T3, indicating cellular uptake of NBD-AT is facilitated to HeLa in a spatiotemporal manner. Since NBD emits relatively strong fluorescence when it enters a hydrophobic environment, several studies exploited the NBD-modified molecule as a powerful tool to investigate supramolecular structure formation inside the cellular organelle,^{25,26,37,38} thus, we exploited NBD-AT as an indicator of self-assembly in cells. After incubating 10 μ M NBD-AT in HeLa for 30 min, we did not observe a green fluorescence (Figure S20), but we observed green fluorescence after the cotreatment of NBD-AT and Pep-AT, which is colocalized with LysoTracker Red. This result indicates that the self-assembly structure of Pep-AT existed in the lysosome.

Collectively, the results suggested that the extracellularly generated nanofiber can be spatiotemporally entrapped into the lysosome via CAIX-mediated endocytosis in HeLa compared to NIH/3T3.

It was hypothesized that the nanofiber for Pep-AT can be activated to interact with the organelle membrane at a positive charge in response to the low pH in the lysosome environment due to the pK_a of acetazolamide. To explore the effect of Pep-AT on the lysosome dynamic, we initially observed the morphology of the lysosome using TEM. As shown in Figure 3a, lysosomes preserve a clear and circular morphology in control HeLa; however, a noticeable swelling was observed in Pep-AT-treated HeLa.³⁹ Additionally, we investigated the lysosome membrane integrity using an acridine orange (AO) dye. The AO dye is a cell-permeable dye that can be accumulated in the lysosome, where green fluorescence is quenched due to protonation, and the green emission intensity is significantly increased when released into a cytosol after lysosomal membrane disruption.⁴⁰ We observed that the AO dye emitted more bright-green fluorescence in Pep-AT-treated HeLa cells, indicating that the nanofiber in the lysosome could disrupt the integrity of the lysosomal membrane (Figure 3b), but constant fluorescence was observed in NIH/3T3 for 20 h after Pep-AT treatment. To perform quantitative analysis, we compared the fluorescence intensity of AO between Pep-AT-treated and untreated groups. It was shown that the intensity of AO increased 3-fold higher in HeLa than in NIH/3T3 (Figure 3c). The overall results suggest that the spatiotemporally lysosome-localized nanofiber can disturb the integrity of the lysosome membrane and surface charge conversion responding to low pH.

Lysosomal disruption can induce cell death. Therefore, this system can be employed in cancer therapy. We performed a cell viability measurement *in vitro* to explore the potential for cancer therapy. The cell viability was measured by a 3-[4,5-dimethylthiazol-2-yl]-2,5 diphenyl tetrazolium bromide (MTT) assay for 24 h. As shown in Figure 3d, we observed concentration-dependent cellular cytotoxicity for Pep-AT toward HeLa compared to NIH/3T3, implying the significance of the spatiotemporal control of the controllable peptide. However, Pep-T exhibited similar cytotoxicity with Pep-AT for HeLa and NIH/3T3 (Figure S21a). We further calculated the selectivity index by dividing the IC_{50} value of NIH/3T3 by the IC_{50} value of HeLa in terms of Pep-AT and Pep-T. The selectivity index for Pep-AT was approximately 2.5-fold higher than for Pep-T (Figure S21b). In addition, there was no cytotoxicity toward HeLa and NIH/3T3 for Pep-A and Pep, indicating that the lack of a bioactive epitope was insufficient to control the cellular fate (Figure S22a,b). To investigate the CAIX-targeting ability of Pep-AT, we measured the cell viability with the pretreatment of acetazolamide as a CAIX inhibitor. We observed that acetazolamide pretreated HeLa was rescued from the cytotoxicity for Pep-AT (Figure S23). CAIX is overexpressed in hypoxic cancer cells;²⁸ we measured the cell viability under a hypoxic condition. As shown in Figure S24, the cytotoxicity gap between HeLa and NIH/3T3 was greater than that under normoxia conditions, indicating that the overexpression of CAIX can facilitate the lysosomal accumulation of Pep-AT. To check the versatility of Pep-AT in addition to HeLa and NIH/3T3, we screened the IC_{50} value for other CAIX-positive/-negative cell lines (Figure S25). We observed that the CAIX-positive cell line (cancer cell lines, red bar) had a low IC_{50} value compared to the CAIX-negative cell

line (normal cell lines, orange bar) (Figure 3e). Finally, we revealed the cell death mechanism using Annexin V-FITC/propidium iodide (PI) staining. We observed green fluorescence from Annexin V-FITC and red fluorescence from PI after Pep-AT incubation for 24 h, suggesting that cellular apoptosis occurred after lysosomal membrane disruption (Figure S26a). To quantitatively analyze the cell death mechanism, we performed flow cytometry analysis toward 20 μ M Pep-AT-treated HeLa. Figure S26b shows that above 90% of the cells enter the apoptotic pathway. Subsequently, we measured the cell viability of Pep-AT with pretreatment of Z-VAD-FMK, which is a known apoptosis inhibitor. It was revealed that Z-VAD-FMK can rescue HeLa cells from cytotoxicity for Pep-AT (Figure S26c). Overall, these results suggest that Pep-AT could be utilized for cancer therapy by directly controlling the cellular fate.

In summary, we described the use of the enzyme-targetable controllable peptide self-assembly system to directly modulate cellular fate with increased interaction with biomacromolecules. We presented a pH-dependent self-assembly behavior and showed molecular-packing change and surface charge conversion. The nanofiber showed a negative surface charge at pH 7.4 because of the deprotonated form of acetazolamide. However, as the pH was adjusted to 4.5, the nanofiber afforded a highly ordered chiral structure, and the molecular charge was changed into a positive charge due to the protonation of acetazolamide. In the cellular environment, the local concentration of the peptide around CAIX gradually increased by the high binding affinity. This allowed the Pep-AT near CAIX to self-assemble into the nanofiber structure, which was spatiotemporally overexpressed in the cancer cell membrane. Following the endocytosis into the lysosome, the nanofiber structure changed in response to the lysosomal environment, and membrane disruption occurred by strong interaction with the positively charged and lipophilic TPP of the nanofiber. This study establishes a novel system to directly regulate cell behavior, exploiting a highly dynamic cellular environment using a pH-responsive peptide self-assembly.

METHODS

Peptide Synthesis and Characterization

The designed peptides were synthesized using standard 9-fluorenylmethoxycarbonyl (Fmoc) solid-phase peptide synthesis (SPPS). Rink amide MBHA resin (0.106 mol) was used as a bead support. Rink amide MBHA resin was swelled in dimethylformamide (DMF) for 30 min, followed by deprotection for Fmoc using a 20% piperidine solution in DMF for 40 min. First, Fmoc-protected amino acid (0.5 mol) was coupled with HBTU (0.45 mol) and DIPEA (1.00 mol) in DMF for 1 h 40 min. Deprotection and amino acid coupling steps were repeated until obtaining a last amino acid conjugation. After deprotection of the last amino acid, 1-pyrenebutyric acid (0.5 mol) was coupled with HBTU (0.45 mol) and DIPEA (1.00 mol) in DMF overnight. For NBD-AT, NBD-NH₂ was coupled instead of 1-pyrenebutyric acid. Next, 4-methyltrityl on a lysine residue was deprotected using 3% TFA in dichloromethane for 30 min two times. Then, 1-hexyl triphenylphosphonium bromide salt (0.04 mmol) with triethyl amine (0.02 mmol) in DMF was reacted with the resin overnight. Then, the peptide was cleaved from the resin using a cleavage cocktail solution (v/v/v of TFA/TIS/H₂O = 95:2.5:2.5) for 3 h. The cleaved peptide was precipitated in cold ether, purified by HPLC, and confirmed by matrix-assisted laser desorption ionization time-of-flight (MALDI-TOF/TOF). To conjugate acetazolamide additionally, purified peptide with 4-oxo-4-((5-sulfamoyl-1,3,4-thiadiazol-2-yl)amino)butanoic acid (Az-COOH, 2 eq), HBTU (1.95 eq), and DIPEA (4 eq) in DMF was allowed to stir overnight. The

crude peptide was purified by HPLC and confirmed by MALDI-TOF/TOF.

UV-Vis, Fluorescence, and CD Spectroscopies

Each peptide solution to analyze was prepared in PBS (10 mM, pH 7.4) or sodium acetate buffer (10 mM, pH 4.5). For UV-vis absorbance, the wavelength range from 300 to 400 nm was recorded with 200 nm/min for scan speed. For fluorescence measurement, the wavelength range from 400 to 600 nm was recorded with 240 nm/min for scan speed ($\lambda_{\text{ex}} = 360$ nm). The slit widths for excitation and emission were set to 10 nm. For CD measurement, the wavelength range from 190 to 400 nm was recorded with 10 nm/min for scan speed.

SEM Measurement

The cell culture Thermanox coverslip with a diameter of 15 mm (Nalge Nunc International, NY) was added into a 24-well plate. HeLa and NIH/3T3 cell lines were seeded into a 24-well plate containing a coverslip with a density of 100,000 per well. After 24 h of growing, the peptide solution diluted in the cell culture medium was incubated for the desired time. For the negative control group, a free medium was added. Then, the medium was removed and cells were washed with 1X PBS and distilled water, sequentially. A coverglass containing the cells was pulled out and immersed in liquid nitrogen. The fully dehydrated coverglass was observed by scanning electron microscopy (SEM).

Cellular Uptake Study

A HeLa cell line was seeded in an 8-well Lab Tek II slide chamber with a density of 10,000 per well. After 24 h of growing, 200 μ M acetazolamide was incubated with the cells for 30 min. For the negative control group, a fresh medium was incubated with the cells. Then, the medium was washed with PBS and exchanged with a medium containing 20 μ M Pep-AT, and the CLSM image was obtained by LSM 780 and 880 by ZEISS.

Cellular TEM Preparation

A HeLa cell line was seeded in a 6-well plate (Thermo Fisher Scientific Inc.) with a density of 300,000 per well. After 24 h of growing, the medium was replaced by a peptide solution diluted into a cell culture medium. After that, the medium was removed and cells were washed with 1X PBS. The cells were harvested using Trypsin-EDTA (0.25%) into a microtube and washed with 0.1 M sodium phosphate buffer with 5% sucrose once. After that, the cells were fixed using 4% paraformaldehyde (PFA) at RT for 30 min. Fixed cells were washed with 0.1 M sodium phosphate buffer with 5% sucrose three times. The cells were postfixed using 1% osmium tetroxide in 0.1 M sodium phosphate buffer with 5% sucrose for 1 h and then washed with distilled water three times. The cells were then dehydrated from water to acetone in a stepwise manner and embedded into an epoxy resin. The epoxy resin was polymerized at 80 °C for 12 h and sliced into ultrathin sections (80 nm) by CR-X ultramicrotome. Ultrathin sections were observed by transmission electron microscopy operating at 120 kV.

Colocalization Study

HeLa and NIH/3T3 cell lines were seeded in an 8-well Lab Tek II slide chamber with a density of 10,000 per well. After 24 h of growing, 20 μ M peptide solution diluted in a cell culture medium was incubated for 30 min. Then, the medium was removed and the cells were incubated with LysoTracker Red DND-99 (Invitrogen) and Mitotracker Green FM (Invitrogen) sequentially following the manufacturer's protocol. The cells were washed with PBS and analyzed using LSM 780 and 880 by ZEISS. The histogram for fluorescence intensity was obtained from ImageJ software (NIH).

Lysosome Membrane Disruption Study

HeLa and NIH/3T3 cell lines were seeded in an 8-well Lab Tek II slide chamber with a density of 10,000 per well. After 24 h of growing, 20 μ M peptide solution diluted in a cell culture medium was incubated for 20 h. Then, the medium was removed and the cells were incubated with an Acridine Orange staining solution (abcam,

ab270791) by following the manufacturer's protocol. The cells were washed with PBS and analyzed using LSM 780 and 880 by ZEISS. The fluorescence intensity ratio was obtained from ImageJ software (NIH).

MTT Assay

For the MTT assay, the cells were seeded in a 96-well plate (Thermo Fisher Scientific Inc.) with a density of 10,000 per well. After growing for 24 h, different concentrations of peptide solutions (0, 10, 20, and 30 μM) were incubated into the cells. After 24 h, 100 μL of MTT solution diluted 10 times with a medium was replaced for 4 h, and MTT was solubilized by 100 μL of SDS-HCl solution for 12 h. The MTT absorbance at 595 nm was measured by a microplate reader. For the hypoxic experiment, a 96-well plate was placed into a hypoxic chamber (1.0% O_2) after seeding the cells. After 24 h of growing, peptide solutions were incubated into the cells under a hypoxic condition. Then, MTT was utilized to check the cell cytotoxicity. All of the experiments were performed in triplicate.

ASSOCIATED CONTENT

Supporting Information

The Supporting Information is available free of charge at <https://pubs.acs.org/doi/10.1021/jacsau.2c00422>.

Experimental procedures; characterization data of products; ^1H NMR spectrum of TPP-C6-Br in CDCl_3 ; ^1H NMR spectrum of Az- NH_2 in $\text{DMSO}-d_6$; mass spectroscopy for Pep-AT, Pep-T, Pep-A, and Pep; purity of synthesized peptides was analysed by HPLC (PDF)

AUTHOR INFORMATION

Corresponding Author

Ja-Hyoung Ryu – Department of Chemistry, Ulsan National Institute of Science and Technology, Ulsan 44919, Republic of Korea; orcid.org/0000-0003-0252-0985; Email: jhyru@unist.ac.kr

Authors

Dohyun Kim – Department of Chemistry, Ulsan National Institute of Science and Technology, Ulsan 44919, Republic of Korea

Sangpil Kim – Department of Chemistry, Ulsan National Institute of Science and Technology, Ulsan 44919, Republic of Korea

Gaeun Park – Department of Chemistry, Ulsan National Institute of Science and Technology, Ulsan 44919, Republic of Korea

Huyeon Choi – Department of Chemistry, Ulsan National Institute of Science and Technology, Ulsan 44919, Republic of Korea

Complete contact information is available at: <https://pubs.acs.org/doi/10.1021/jacsau.2c00422>

Author Contributions

[‡]D.K. and S.K. contributed equally to this work. CRediT: Dohyun Kim investigation, writing-original draft, writing-review & editing; Sangpil Kim investigation, writing-review & editing; Gaeun Park investigation; Huyeon Choi investigation; Ja-Hyoung Ryu conceptualization, project administration, supervision, writing-original draft, writing-review & editing.

Notes

The authors declare no competing financial interest.

ACKNOWLEDGMENTS

This work was supported by the National Research Foundation of Korea (NRF) grants funded by the Korean Government (MSIT) (2020R1A2C3005939 and 2020M3A9D8038192). The authors thank UCRF (UNIST Central Research Facilities) for allowing use of their equipment.

REFERENCES

- (1) Demaurex, N. pH Homeostasis of Cellular Organelles. *Physiology* **2002**, *17*, 1–5.
- (2) Lagadic-Gossmann, D.; Huc, L.; Lecreur, V. Alterations of intracellular pH homeostasis in apoptosis: origins and roles. *Cell Death Differ.* **2004**, *11*, 953–961.
- (3) Shen, J.; Zeng, Y.; Zhuang, X.; Sun, L.; Yao, X.; Pimpl, P.; Jiang, L. Organelle pH in the Arabidopsis Endomembrane System. *Mol. Plant* **2013**, *6*, 1419–1437.
- (4) Michl, J.; Park, K. C.; Swietach, P. Evidence-based guidelines for controlling pH in mammalian live-cell culture systems. *Commun. Biol.* **2019**, *2*, No. 144.
- (5) Conus, S.; Simon, H.-U. Cathepsins: Key modulators of cell death and inflammatory responses. *Biochem. Pharmacol.* **2008**, *76*, 1374–1382.
- (6) Ishidoh, K.; Kominami, E. Processing and activation of lysosomal proteinases. *Biol. Chem.* **2002**, *383*, 1827–1831.
- (7) Chen, S.; Dong, H.; Yang, S.; Guo, H. Cathepsins in digestive cancers. *Oncotarget* **2017**, *8*, 41690–41700.
- (8) Chwieralski, C. E.; Welte, T.; Bühling, F. Cathepsin-regulated apoptosis. *Apoptosis* **2006**, *11*, 143–149.
- (9) Cheung, A. Y.; de Vries, S. C. Membrane trafficking: intracellular highways and country roads. *Plant Physiol.* **2008**, *147*, 1451–1453.
- (10) Zhang, Y.; Moss, A.; Tan, K.; Herr, A. E. Barcodes for subcellular protein localization. *Nat. Biomed. Eng.* **2019**, *3*, 673–675.
- (11) Saftig, P.; Klumperman, J. Lysosome biogenesis and lysosomal membrane proteins: trafficking meets function. *Nat. Rev. Mol. Cell Biol.* **2009**, *10*, 623–635.
- (12) Wang, G.-Q.; Yang, J.; Hou, D.-Y.; Zheng, R.; Mamuti, M.; Guo, M.-J.; Fan, Z.; An, H.-W.; Wang, H. Conformational Transition-Triggered Disassembly of Therapeutic Peptide Nanomedicine for Tumor Therapy. *Adv. Healthcare Mater.* **2021**, *10*, No. 2100333.
- (13) Wang, J.; Hu, L.; Zhang, H.; Fang, Y.; Wang, T.; Wang, H. Intracellular Condensates of Oligopeptide for Targeting Lysosome and Addressing Multiple Drug Resistance of Cancer. *Adv. Mater.* **2022**, *34*, No. 2104704.
- (14) Kim, S.; Yoon, N. G.; Jana, B.; Kang, B. H.; Ryu, J.-H. Quaternary ammonium-based mitochondria targeting anticancer agents with high water solubility. *Bull. Korean Chem. Soc.* **2022**, *43*, 391–395.
- (15) Zhang, Y.; Gao, Q.; Li, W.; He, R.; Zhu, L.; Lian, Q.; Wang, L.; Li, Y.; Bradley, M.; Geng, J. Controlled Intracellular Polymerization for Cancer Treatment. *JACS Au* **2022**, *2*, 579–589.
- (16) Zhou, J.; Du, X.; Berciu, C.; He, H.; Shi, J.; Nicastro, D.; Xu, B. Enzyme-Instructed Self-Assembly for Spatiotemporal Profiling of the Activities of Alkaline Phosphatases on Live Cells. *Chem* **2016**, *1*, 246–263.
- (17) He, H.; Liu, S.; Wu, D.; Xu, B. Enzymatically Formed Peptide Assemblies Sequester Proteins and Relocate Inhibitors to Selectively Kill Cancer Cells. *Angew. Chem., Int. Ed.* **2020**, *59*, 16445–16450.
- (18) Yuan, Y.; Zhang, J.; Qi, X.; Li, S.; Liu, G.; Siddhanta, S.; Barman, I.; Song, X.; McMahon, M. T.; Bulte, J. W. M. Furin-mediated intracellular self-assembly of olsalazine nanoparticles for enhanced magnetic resonance imaging and tumour therapy. *Nat. Mater.* **2019**, *18*, 1376–1383.
- (19) Yang, L.; Peltier, R.; Zhang, M.; Song, D.; Huang, H.; Chen, G.; Chen, Y.; Zhou, F.; Hao, Q.; Bian, L.; He, M.; Wang, Z.; Hu, Y.; Sun, H. Desuccinylation-Triggered Peptide Self-Assembly: Live Cell Imaging of SIRT5 Activity and Mitochondrial Activity Modulation. *J. Am. Chem. Soc.* **2020**, *142*, 18150–18159.

- (20) Kalafatovic, D.; Nobis, M.; Javid, N.; Frederix, P. W. J. M.; Anderson, K. I.; Saunders, B. R.; Uljin, R. V. MMP-9 triggered micelle-to-fibre transitions for slow release of doxorubicin. *Biomater. Sci.* **2015**, *3*, 246–249.
- (21) Sundelacruz, S.; Levin, M.; Kaplan, D. L. Role of membrane potential in the regulation of cell proliferation and differentiation. *Stem Cell Rev. Rep.* **2009**, *5*, 231–246.
- (22) Casares, D.; Escribá, P. V.; Rosselló, C. A. Membrane Lipid Composition: Effect on Membrane and Organelle Structure, Function and Compartmentalization and Therapeutic Avenues. *Int. J. Mol. Sci.* **2019**, *20*, No. 2167.
- (23) Cheng, D.-B.; Zhang, X.-H.; Gao, Y.-J.; Ji, L.; Hou, D.; Wang, Z.; Xu, W.; Qiao, X.-Y.; Wang, H. Endogenous Reactive Oxygen Species-Triggered Morphology Transformation for Enhanced Cooperative Interaction with Mitochondria. *J. Am. Chem. Soc.* **2019**, *141*, 7235–7239.
- (24) Newcomb, C. J.; Sur, S.; Ortony, J. H.; Lee, O.-S.; Matson, J. B.; Boekhoven, J.; Yu, J. M.; Schatz, G. C.; Stupp, S. I. Cell death versus cell survival instructed by supramolecular cohesion of nanostructures. *Nat. Commun.* **2014**, *5*, No. 3321.
- (25) Jeena, M. T.; Palanikumar, L.; Go, E. M.; Kim, I.; Kang, M. G.; Lee, S.; Park, S.; Choi, H.; Kim, C.; Jin, S.-M.; Bae, S. C.; Rhee, H. W.; Lee, E.; Kwak, S. K.; Ryu, J.-H. Mitochondria localization induced self-assembly of peptide amphiphiles for cellular dysfunction. *Nat. Commun.* **2017**, *8*, No. 26.
- (26) Kim, S.; Jana, B.; Go, E. M.; Lee, J. E.; Jin, S.; An, E.-K.; Hwang, J.; Sim, Y.; Son, S.; Kim, D.; Kim, C.; Jin, J.-O.; Kwak, S. K.; Ryu, J.-H. Intramitochondrial Disulfide Polymerization Controls Cancer Cell Fate. *ACS Nano* **2021**, *15*, 14492–14508.
- (27) Fisher, S. Z.; Aggarwal, M.; Kovalevsky, A. Y.; Silverman, D. N.; McKenna, R. Neutron Diffraction of Acetazolamide-Bound Human Carbonic Anhydrase II Reveals Atomic Details of Drug Binding. *J. Am. Chem. Soc.* **2012**, *134*, 14726–14729.
- (28) Jung, H. S.; Han, J.; Shi, H.; Koo, S.; Singh, H.; Kim, H.-J.; Sessler, J. L.; Lee, J. Y.; Kim, J.-H.; Kim, J. S. Overcoming the Limits of Hypoxia in Photodynamic Therapy: A Carbonic Anhydrase IX-Targeted Approach. *J. Am. Chem. Soc.* **2017**, *139*, 7595–7602.
- (29) Li, J.; Shi, K.; Sabet, Z. F.; Fu, W.; Zhou, H.; Xu, S.; Liu, T.; You, M.; Cao, M.; Xu, M.; Cui, X.; Hu, B.; Liu, Y.; Chen, C. New power of self-assembling carbonic anhydrase inhibitor: Short peptide-constructed nanofibers inspire hypoxic cancer therapy. *Sci. Adv.* **2019**, *5*, No. eaax0937.
- (30) Kim, J. H.; Verwilt, P.; Won, M.; Lee, J.; Sessler, J. L.; Han, J.; Kim, J. S. A Small Molecule Strategy for Targeting Cancer Stem Cells in Hypoxic Microenvironments and Preventing Tumorigenesis. *J. Am. Chem. Soc.* **2021**, *143*, 14115–14124.
- (31) Hu, Y.; Lin, R.; Zhang, P.; Fern, J.; Cheetham, A. G.; Pater, K.; Schulman, R.; Kan, C.; Cui, H. Electrostatic-Driven Lamination and Untwisting of β -Sheet Assemblies. *ACS Nano* **2016**, *10*, 880–888.
- (32) Su, H.; Wang, F.; Wang, H.; Zhang, W.; Anderson, C. F.; Cui, H. Propagation-Instigated Self-Limiting Polymerization of Multi-armed Amphiphiles into Finite Supramolecular Polymers. *J. Am. Chem. Soc.* **2021**, *143*, 18446–18453.
- (33) Xing, H.; Chin, S. M.; Udumula, V. R.; Krishnaiah, M.; Almeida, N. R.; Huck-Iriart, C.; Picco, A. S.; Lee, S. R.; Zaldivar, G.; Jackson, K. A.; Tagliacuzzi, M.; Stupp, S. I.; Conda-Sheridan, M. Control of Peptide Amphiphile Supramolecular Nanostructures by Isosteric Replacements. *Biomacromolecules* **2021**, *22*, 3274–3283.
- (34) Hestand, N. J.; Spano, F. C. Expanded Theory of H- and J-Molecular Aggregates: The Effects of Vibronic Coupling and Intermolecular Charge Transfer. *Chem. Rev.* **2018**, *118*, 7069–7163.
- (35) Zheng, R.; Yang, J.; Mamuti, M.; Hou, D.-Y.; An, H.-W.; Zhao, Y.; Wang, H. Controllable Self-Assembly of Peptide-Cyanine Conjugates In Vivo as Fine-Tunable Theranostics. *Angew. Chem., Int. Ed.* **2021**, *60*, 7809–7819.
- (36) Sorrenti, A.; Leira-Iglesias, J.; Markvoort, A. J.; de Greef, T. F. A.; Hermans, T. M. Non-equilibrium supramolecular polymerization. *Chem. Soc. Rev.* **2017**, *46*, 5476–5490.
- (37) Mazères, S.; Schram, V.; Tocanne, J.-F.; Lopez, A. 7-nitrobenzo-2-oxa-1,3-diazole-4-yl-labeled phospholipids in lipid membranes: differences in fluorescence behavior. *Biophys. J.* **1996**, *71*, 327–335.
- (38) Gao, Y.; Shi, J.; Yuan, D.; Xu, B. Imaging enzyme-triggered self-assembly of small molecules inside live cells. *Nat. Commun.* **2012**, *3*, No. 1033.
- (39) Hu, L.; Li, Y.; Lin, X.; Huo, Y.; Zhang, H.; Wang, H. Structure-Based Programming of Supramolecular Assemblies in Living Cells for Selective Cancer Cell Inhibition. *Angew. Chem., Int. Ed.* **2021**, *60*, 21807–21816.
- (40) Bonam, S. R.; Wang, F.; Muller, S. Lysosomes as a therapeutic target. *Nat. Rev. Drug Discovery* **2019**, *18*, 923–948.